Early pathological amyloid induces hypersynchrony of BOLD resting-state networks in transgenic mice and provides an early therapeutic window before amyloid plaque deposition

by

Disha Shah, Jelle Praet, Amira Latif Hernandez, Corinna Höfling, Cynthia Anckaerts, Frédérique Bard, Markus Morawski, Jan R. Detrez, Els Prinsen, Alessandro Villa, Winnok H. De Vos, Adriana Maggi, Rudi D'Hooge, Detlef Balschun, Steffen Rossner, Marleen Verhoye, Annemie Van der Linden

Published in Alzheimers Dement. 2016 Sep;12(9):964-76.

doi: 10.1016/j.jalz.2016.03.010

Title: Early pathological amyloid induces hypersynchrony of BOLD resting-state networks in transgenic mice and provides an early therapeutic window before amyloid plaque deposition

Authors:

Disha Shah[1], Jelle Praet[1*], Amira Latif Hernandez[2*], Corinna Höfling[3], Cynthia Anckaerts[1], Frédérique Bard[4], Markus Morawski[3], Jan R. Detrez[5], Els Prinsen[6], Alessandro Villa[7], Winnok H. De Vos[5,8], Adriana Maggi[7], Rudi D'Hooge[2], Detlef Balschun[2], Steffen Rossner[3], Marleen Verhoye[1], Annemie Van der Linden[1]

*contributed equally to this work.

Authors affiliations:

[1] Bio-Imaging Lab, University of Antwerp, Universiteitsplein 1, 2610 Wilrijk, Antwerp Belgium.

[2] Laboratory of Biological Psychology, Tiensestraat 102 - box 3714, 3000 Leuven, Belgium

[3] Paul Flechsig Institute for Brain Research Liebigstrasse 19, 04103 Leipzig, Germany

[4] Janssen Alzheimer Immunotherapy, South San Francisco, CA, USA.

[5]Laboratory of Cell Biology and Histology, University of Antwerp, Groenenborgerlaan 171, 2020 Antwerp, Belgium.

[6] Department of Biology, University of Antwerp, Groenenborgerlaan 171, 2020 Antwerp, Belgium.

[7] Center of Excellence on Neurodegenerative Diseases and Department of Pharmacological and Biomolecular Sciences, University of Milan, 20133, Milan, Italy.

[8] Cell Systems and Imaging, Department Molecular Biotechnology, University of Ghent, Coupure links 653, 9000 Ghent, Belgium.

Corresponding author:

Disha Shah

Bio-Imaging Lab, University of Antwerp, Universiteitsplein 1, 2610 Wilrijk, Antwerp Belgium

email: Disha.Shah@uantwerpen.be

Phone: + 32 (0)3 265.27.62.

Abstract

INTRODUCTION: In Alzheimer's disease (AD), pathological amyloid-beta (Aβ) is synaptotoxic and impairs neuronal function at the microscale, influencing brain networks at the macroscale before Aβ deposition. The latter can be detected non-invasively, *in vivo*, using resting-state-functional MRI (rsfMRI), a technique used to assess brain functional connectivity (FC).

METHODS: RsfMRI was performed longitudinally in TG2576 and PDAPP mice, starting before Aβ deposition to determine the earliest FC changes. Additionally, the role of pathological Aβ on early FC alterations was investigated by treating TG2576 mice with the 3D6 anti-Aβ-antibody.

RESULTS: Both transgenic models showed hypersynchronized FC before Aβ deposition and hyposynchronized FC at later stages. Early anti-Aβ treatment in TG2576 mice prevented hypersynchronous FC, and the associated synaptic impairments and excitatory/inhibitory disbalances.

DISCUSSION: Hypersynchrony of FC may be used as a new non-invasive read-out of early AD and can be recovered by anti-Aβ treatment, encouraging preventive treatment strategies in familial AD.

1. Introduction

Alzheimer's disease (AD) is a progressive neurodegenerative disorder, characterized by deficits in learning, memory and cognitive function [1]. The pathological hallmarks of AD include the progressive accumulation of extracellular amyloid plaques and intracellular tangles.

The amyloid cascade hypothesis postulates that abnormal accumulation of amyloid-beta (Aβ), one of the earliest events in AD pathology, triggers the formation of tau tangles and neurodegeneration, eventually resulting in the clinical expression of AD [2,3]. The non-linear correlation between Aβ plaque deposition and dementia has led to a shift of the amyloid cascade hypothesis towards the soluble form of Aβ, which exerts synaptotoxic and neurotoxic effects [4]. Indeed, several transgenic mouse models of amyloidosis show cognitive dysfunctions and impaired synaptic functioning before the manifestation of Aβ plaques [5-11] supporting a destructive role of soluble Aβ on neurological processes that underlie learning and memory.

Synaptic dysfunction elicited by soluble Aβ leads to impaired communication between brain regions, resulting in deficits of neuronal networks which could be expressed as cognitive disturbances [4,12]. The non-invasive detection of such network alterations would allow elucidating the spatiotemporal relation between amyloid pathology and functional impairments and provide a tool for early diagnosis. Alterations at the neuronal network level can be detected non-invasively using resting-state functional Magnetic Resonance Imaging (rsfMRI). In rsfMRI, low frequency (0.01-0.1Hz) fluctuations of the blood-oxygenation-level-dependent (BOLD) signal are considered to reflect underlying fluctuations of neuronal activity. Functional connectivity (FC) is defined as the temporal correlation of BOLD-fluctuations between spatially distinct brain regions [13].

RsfMRI has been applied to study functional disruptions in AD patients [14] and to a lesser extent in mouse models of amyloidosis [15]. These studies showed FC impairments between brain regions important for learning and memory following Aβ plaque deposition. However, the ability to non-invasively detect early-stage FC changes in mouse models of amyloidosis, thus when no plaques are present yet, would open doors in terms of early diagnosis. The current study longitudinally

investigated BOLD FC networks in two transgenic mouse models of amyloidosis at a pre-plaque stage, i.e. the TG2576 [16] and PDAPP mice [17].

2. Material and methods

2.1. Ethical statement

All procedures were performed in strict accordance with the European Directive 2010/63/EU on the protection of animals used for scientific purposes. The protocols were approved by the Committee on Animal Care and Use at the University of Antwerp, Belgium (permit numbers 2013-62 and 2015-07) and all efforts were made to minimize animal suffering.

2.2. Animals

2.2.1. Characterization studies

The TG2576 mouse model of amyloidosis (kindly provided by Karen Hsiao Ashe, University of Minnesota) overexpresses the mutant form of APP carrying the Swedish mutation (KM670/671NL) controlled by the hamster prion protein promoter [16]. Aβ plaque development starts at the age of 9-11 months [16]. Female mice were assessed with rsfMRI at the age of 3 months (TG2576 N=10, wild-type N=13), 5 months (TG2576 N=10, wild-type N=12), 8 months (TG2576 N=9, wild-type N=12), 14 months (TG2576 N=9, wild-type N=9) and 18 months (TG2576 N=11, wild-type N=12). At each time point, TG2576 and wild-type mice were sacrificed for immunohistochemistry to assess Aβ plaques (thioflavin-S), astrocytosis (GFAP) and microgliosis (Iba1) (TG2576 N=4/ age group, wild type N=2/ age group). Immunofluorescence analyses were performed according to a previously described protocol [18]. Additional analyses were performed in 5 months old TG2576 and wild-type mice: Synaptic plasticity was assessed using electrophysiology (N=6/group) as described previously [19], real time reverse transcription (RT)-qPCR was performed to assess microglial markers (Iba1, interleukin-1β, macrophage inflammatory protein, interleukin-10, arginase-1 and chitinase-like-3, N=5/group), and ELISA was used to determine the level of soluble Aβ (N=4/group). For a detailed description of immunohistochemistry, electrophysiology, RT-qPCR and ELISA procedures cfr. Supplementary methods.

The PDAPP mouse model of amyloidosis (kindly provided by Janssen Alzheimer Immunotherapy, South San Francisco, CA, USA) overexpresses the mutant form of APP carrying the Indiana mutation (V717F) controlled by the PDGF promotor [17]. These mice start to develop Aβ plaques around the age of 8-9 months. In this study female mice were evaluated with rsfMRI at 3 months (PDAPP N=20, wild-type N=20) of age, after which a subgroup of mice was sacrificed for immunohistochemistry and ELISA (N=4/group), to assess Aβ plaques (thioflavin-S) and soluble Aβ respectively. The remaining mice were scanned with rsfMRI again at 5 months (PDAPP N=16, wild-type N=15) and 7 months of age (PDAPP N=16, wild-type N=15). For a detailed description of immunohistochemistry and ELISA procedures cfr. Supplementary methods.

2.2.2. Treatment study

TG2576 and wild-type mice (N=40/group) were scanned with rsfMRI at 3 months of age, after which they were divided into 4 treatment groups (N=20/group) i.e. wild-type and TG2576 shams and wild-type and TG2576 treated. The sham groups received a weekly intraperitoneal (i.p.) injection of 0.02 ml/kg body weight (BW) phosphate buffered saline (PBS, injected volume 0.5ml) and the treated groups received 10mg/kg BW (injected volume 0.5ml) 3D6 antibody (kindly provided by Janssen Alzheimer Immunotherapy, South San Francisco, CA, USA) to clear Aβ. The treatment regimen started when all mice were 3 months of age and lasted 10 weeks, after which all mice were scanned again with rsfMRI. After the rsfMRI scans a subgroup of mice was sacrificed for immunohistochemistry to assess glutamatergic (VGLUT-1) synapses, GABAergic (GAD65-67) synapses, and presynaptic (synapsin) and postsynaptic (synaptobrevin) markers (N=4/group), electrophysiological analyses to investigate synaptic plasticity (N=6/group), and ultra-performance liquid chromatography tandem mass spectrometry (UPLC-MS/MS, N=4/group) to determine the ratio of glutamate/GABA neurotransmitters. The remaining mice (N=10/group) were scanned again with rsfMRI at 7, 8 and 10 months of age. For a detailed description of immunohistochemistry, electrophysiology and UPLC-MS/MS procedures cfr. Supplementary methods.

2.3. MRI procedures

For MRI handling procedures, mice were anesthetized with 2% isoflurane. During the rsfMRI measurements, a combination of isoflurane (0.4%) and medetomidine (0.3mg/kg) was used to sedate the animals as described previously [20]. Breathing rate, heart rate, blood oxygenation and body temperature were monitored throughout the MRI procedure. MRI scans were performed on a 9.4T Biospec MRI system and images were acquired using a standard Bruker crosscoil set-up using a quadrature volume coil and a quadrature surface coil designed for mice. Three orthogonal multi-slice Turbo RARE T2-weighted images were acquired to render slice-positioning uniform (repetition time 2000 ms, echo time 15 ms, 16 slices of 0.4 mm). Field maps were acquired for each animal to assess field homogeneity, followed by local shimming, which corrects for the measured inhomogeneity in a rectangular volume within the brain. RsfMRI signals were measured by a T_2*-weighted single shot echo-planar-imaging (EPI) sequence (repetition time 2000 ms, echo time 15 ms, 16 slices of 0.4mm, 150 repetitions). The field-of-view was (20 x 20) mm^2 and the matrix size (128 x 64), resulting in voxel dimensions of (0.156 x 0.312 x 0.4) mm^3. RsfMRI preprocessing was performed as described previously [15]. Independent component analysis (ICA) was performed in 3 months old wild type animals to determine which brain networks can be discerned. Next, the regions that were part of the neurologically relevant ICA components (**Supplementary Table 1**) were used for region-of-interest (ROI) correlation analyses, which resulted in FC matrices. Additionally, individual z-transformed FC-maps were obtained for all animals with the right hippocampus as seed region. For a detailed description of MRI procedures and processing cfr. Supplementary methods.

2.4. Statistical analyses

Statistical analyses of FC strength per brain network and electrophysiological recordings included a two way ANOVA, with the Holm-Sidak correction for multiple comparisons ($p<0.05$). Statistical analyses of the zFC-maps include a one sample T-test for within group analyses , a two sample T-test for comparison between two groups and a one way ANOVA for comparison between multiple groups, with the false discovery rate (FDR) correction for multiple comparisons ($p<0.05$) and a threshold of

minimum 10 voxels. Statistical analyses of the immunohistochemical stainings were performed using the Kruskal-Wallis test with the Dunn's correction for multiple comparisons ($p<0.05$). Reported values are mean ± standard error.

3. Results

3.1. BOLD rsfMRI shows pre-plaque stage hypersynchrony in TG2576 mice

BOLD FC was assessed in TG2576 mice before (3, 5 and 8 months) and after Aβ plaque deposition (14 and 18 months). **Figure 1** shows BOLD FC strength matrices of TG2576 and age-matched wild-types at each time point. The networks that were assessed are presented in **Supplementary Figure 1,** which shows the neurological ICA components observed in 3 months old wild-type animals i.e. the hippocampus, default-mode-like (DMN-like), cingulate, frontal, caudate putamen, sensorimotor, frontal-thalamus and piriform networks. At 5 months of age, TG2576 mice showed hypersynchronous BOLD FC compared to age-matched wild-type littermates. Starting from 8 until 18 months of age, BOLD FC decreased in TG2576 mice compared to wild-type mice. **Figure 2A** shows that the hippocampus network demonstrated a trend towards hypersynchrony of BOLD FC as early as 3 months of age ($p=0.07$). At 5 months of age hypersynchrony of BOLD FC was more extensive, and most significant in the hippocampus ($p=0.0004$). Additionally, hypersynchronous BOLD FC was observed in the DMN-like network ($p=0.029$), and a trend was observed in the cingulate network and frontal-thalamus network. **Figure 2B** shows that hippocampus BOLD FC strength was decreased in TG2576 mice compared to wild-types at 8 months of age ($p=0.044$) and 18 months of age ($p<0.0001$). The evolution of BOLD FC over time is shown for each network in **Supplementary Figure 2**. **Figure 2C** shows a seed-based analysis of the right hippocampus, which confirmed hypersynchronous BOLD FC in the hippocampus of 5 months old TG2576 mice ($p=0.031$).

Immunohistochemistry in the hippocampus of 5 months old TG2576 and wild-type mice demonstrated no detectable increase in astrocytosis (GFAP) or microgliosis (Iba-1) (**Figure 3A**). Using qPCR, mRNA expression of the following inflammatory markers was assessed, and no difference was observed between TG2576 and wild-type mice (**Figure 3B**): Iba-1, arginase-1 (Arg-1), interleukin 1b

(IL-1b), macrophage inflammatory protein 2 (MIP-2), interleukin 10 (IL-10), and chitinase 3-like-3 (Chi-3l3). Aβ plaques (thioflavin-S) were not yet detectable (**Figure 3C**), but ELISA (**Figure 3C**) showed an increase in soluble Aβ load in the TG2576 mice (1520 ± 80 pg/ml) compared to wild-type mice (129 ± 13 pg/ml). Immunohistochemistry of astrocytes (GFAP), microglia (Iba-1) and amyloid plaques (thioflavin-S) is shown for each time point in **Supplementary Figure 3**.

To characterize changes in synaptic functioning in 5 months old TG2576 mice, field recordings of paired-pulse responses and long-term potentiation were performed in the hippocampus CA1-region. No significant differences were observed in basal synaptic transmission by stimulation of the Schaffer collateral-CA1 pathway when comparing TG2575 and wild-type mice (**Figure 3D**). Thereafter, paired-pulse facilitation (PPF) was inspected, a phenomenon that reflects presynaptically mediated short-term plasticity. While at most inter-stimulus intervals no genotype difference was detectable, PPF was significantly decreased in TG2576 mice at 200 ms (p=0.03) compared to wild-types (**Figure 3E**). Finally, long-term potentiation (LTP) was measured, an established correlate of learning and memory at the cellular level, and no significant difference was observed between TG2576 and wild-type mice (**Figure 3F**).

3.2. BOLD rsfMRI shows pre-plaque stage hypersynchrony in PDAPP mice

To demonstrate that the observation of hypersynchronous BOLD FC is independent of the hAPP transgenic mouse model, PDAPP mice were subjected to rsfMRI at the age of 3 months i.e. 3-5 months before the appearance of amyloid plaques. The FC matrices in **Figure 4A** reveal that PDAPP mice show increased FC compared to their wild-type littermates. Hypersynchronized BOLD FC was most significant in the frontal network (p=0.04) (**Figure 4B**). At 7 months of age, the frontal network showed decreased BOLD FC in PDAPP versus wild-type mice (p=0.037) (**Figure 4C**). At 3 months of age no Aβ plaques were detected (**Figure 4D**), but ELISA showed an increase in soluble Aβ load in PDAPP mice (721 ± 44.7 pg/ml) compared to wild-type mice (82 ± 6.3 pg/ml) (**Figure 4D**).

3.3. Neutralizing Aβ prevents BOLD hypersynchrony and synaptic deficits in TG2576 mice

Next, TG2576 mice were treated with the 3D6 anti-Aβ–antibody to further investigate the role of pathological Aβ in the observed hypersynchrony of FC. The FC matrices in **Figure 5A** show that treatment with 3D6 recovered FC hypersynchrony and FC patterns were rendered comparable to wild-type mice. This was confirmed by seed-based analyses of the right hippocampus (**Figure 5B**), which demonstrates hypersynchronous BOLD FC in PBS treated TG2576 animals compared to wild-type animals ($p=0.016$), while the 3D6 treated TG2576 mice showed BOLD FC patterns comparable those in wild-types.

The data shown in **Figure 6A** confirms hypersynchronous BOLD FC in the hippocampus of PBS treated TG2576 mice compared to wild-types ($p<0.0001$), while the TG2576 group that received the 3D6 antibody showed BOLD FC that was comparable to wild-type mice. At 8 months of age, i.e. 3 months after the treatment was concluded, PBS treated TG2576 mice showed decreased BOLD FC compared to wild-types, while 3D6 treated TG2576 mice still showed BOLD FC comparable to wild-types. Interestingly, at 10 months of age, i.e. 5 months after the treatment was concluded, PBS treated TG2576 mice still showed lower levels of BOLD FC compared to wild-types, while 3D6 treated TG2576 mice demonstrated hypersynchrony of BOLD FC compared to wild-types ($p=0.003$).

Additionally, 3D6 treated TG2576 mice displayed a rescue of impaired PPF at 200 ms while the same antibody treatment had no effect in wild-type mice at 5 months of age **(Figure 6B)**. Consistent with the findings reported above, PPF of PBS-treated TG2576 mice was significantly reduced at 200 ms ($p=0.004$).

Immunohistochemistry (**Figure 6C**) revealed that the density (puncta/µm²) of VGLUT1 was significantly increased in PBS treated TG2576 compared to wild-types ($p=0.02$), while 3D6 treated TG2576 mice were comparable to wild-types ($p=0.67$). On the other hand, the density (puncta/µm²) of GAD65/67 was significantly decreased in PBS treated TG2576 compared to wild-types ($p=0.03$), but not in 3D6 treated TG2576 mice ($p=0.99$). Thus, the ratio of excitatory (VGLUT1) to inhibitory (GAD-65/67) synapses was significantly increased in the hippocampus of PBS treated TG2576 mice

(p=0.01), while 3D6 treated TG2576 mice showed a VGLUT/GAD-65/67 ratio comparable to wild-types (p=0.99). Similarly, the ratio of glutamate/GABA neurotransmitters was significantly increased in the hippocampus of PBS treated TG2576 mice (p=0.02), but 3D6 treated TG2576 mice were comparable to wild-types (p=0.44) (**Figure 6D**). Additionally, the density (puncta/μm²) of the pre-synaptic marker synapsin was significantly increased in PBS treated TG2576 mice compared to wild-types (p=0.04), but not in 3D6 treated TG2576 mice (p=0.99) (**Figure 6E**). The density (puncta/μm²) of the post-synaptic marker synaptobrevin was not altered.

4. Discussion

This study investigated BOLD FC patterns at early stages of AD progression in transgenic mice. Hypersynchronous BOLD FC was observed before Aβ plaque deposition in two mouse models of amyloidosis i.e. the TG2576 and PDAPP mice. Early treatment of TG2576 mice with an anti-Aβ-antibody prevented hypersynchronous BOLD FC, as well as the associated synaptic impairments and excitatory/inhibitory disbalances.

The TG2576 and PDAPP mouse models of amyloidosis develop Aβ plaques between 9-11 months and 8-9 months of age, respectively [16,17]. Both mouse models show cognitive disturbances and synaptic deficits prior to Aβ plaque deposition [6,7,11,21], suggesting that soluble Aβ, rather than Aβ plaques, are responsible for the observed functional deficits. In the current study TG2576 mice were characterized in terms of BOLD FC using rsfMRI. The results showed hypersynchronous BOLD FC in the hippocampus of TG2576 mice compared to wild-types at 5 months of age, when soluble Aβ was increased, but no Aβ plaques or increased inflammatory responses were detected. Starting from 8 months, BOLD FC decreased in TG2576 mice, which is consistent with the observed hyposynchronous BOLD FC in memory-related regions in AD patients [14] and our previous study in old APP/PS1 mice [15]. The observation of hypersynchronous BOLD FC is consistent with several reports of hyperactive and hypersynchronous neurons associated with Aβ. Busche and colleagues reported hippocampal hyperactivity and hypersynchrony in mouse models of amyloidosis using two-photon Ca^{2+} imaging, and showed that neuronal hyperactivity was caused by increased levels of

soluble Aβ [12,22,23]. This observation was confirmed in a recent study in the TG2576 model [24]. Our results suggest that pre-plaque stage pathological amyloidosis, which could include an accumulation of soluble Aβ, the overexpression of human APP and/or the accumulation of different APP fragments, is associated with hypersynchrony of BOLD FC.

Additionally, hypersynchronous BOLD FC was confirmed in the frontal network of PDAPP mice at 3 months of age, i.e. when there were no Aβ plaques but soluble Aβ was increased. These results suggest that the observation of hypersynchronous BOLD FC itself is not model-specific, but might be attributed to pre-plaque soluble Aβ, human APP and/or different APP fragments. Additionally, the pattern of early hypersynchronous BOLD FC and subsequent hyposynchronous BOLD FC at later stages of disease progression, as observed for the TG2576 mice, was also reproduced in the PDAPP mice. The discrepancy in region-specific vulnerability to amyloid pathology between the TG2576 and PDAPP models might be explained by the fact that both mouse models carry a different mutation i.e. the APP KM670/671NL (Swedish) mutation controlled by the hamster prion protein promotor and APP V717F (Indiana) mutation controlled by the PDGF promotor in TG2576 and PDAPP mice, respectively. Another important difference is that both mouse models are created on different background strains i.e. a mixed C57BL6/SJL and C57BL6/Swiss-Webster/DBA background for TG2576 and PDAPP mice, respectively. A previous study in our group showed that different strains of mice presented a different regional pattern of BOLD FC and glucose metabolism [20]. These differences might result in a different regional vulnerability to amyloid pathology and thus a different spatiotemporal relation between amyloidosis and BOLD FC. In summary, our results strongly suggest that early stages of AD progression are associated with hypersynchrony of BOLD FC networks, before the presence of plaques. Importantly, the current study demonstrates that hypersynchronous neuronal activity, which until now has been reported in several transgenic models of amyloidosis using relatively invasive techniques, can be detected non-invasively, in vivo, with rsfMRI.

It is important to note that while our data show hypersynchronous BOLD FC, Grandjean and colleagues [25] demonstrated hyposynchronous BOLD FC before Aβ plaque deposition in the Arc-Aβ mouse model. This discrepancy could be explained by the fact that they used isoflurane to anesthetize

the animals. Isoflurane is a known vasodilator and thus might influence the BOLD signal. Moreover, since isoflurane targets the GABA-ergic system, it might affect the excitatory/inhibitory disbalances known to occur in amyloidosis models [23]. The fact that we observed hypersynchronous BOLD FC in two different mouse models of amyloidosis is encouraging and suggests that the observation is not model specific. Moreover, it is important to mention that a recent study showed increased BOLD FC in children carrying the presenilin1 (PSEN1) mutation compared to non-carriers [26], which strongly point towards a potential translational value of our findings.

To further investigate the involvement of pathological Aβ in the observed hypersynchronous BOLD FC, TG2576 mice were treated with the 3D6 anti-Aβ-antibody. 3D6, the murine form of bapineuzimab, recognizes amino acids 1-5 of Aβ. It binds to the N-terminal of Aβ and does not recognize other hAPP fragments [27]. Studies have shown that 3D6 enters the central nervous system upon systemic injection [28-30], binds soluble Aβ [31,32] and improved behaviour and synaptic impairments in amyloidosis models [31]. Treatment with the 3D6 antibody rescued hypersynchrony of BOLD FC in TG2576 mice at 5 months. Follow-up of the treated mice until 8 months of age, so 3 months after the treatment was concluded, showed that early treatment does not only prevent the hypersynchrony of BOLD FC at 5 months, but also subsequent hyposynchrony of BOLD FC in TG2576 mice at 8 months of age. Our results strongly suggest that an early treatment might rescue or delay the effect of pathological Aβ on brain function. A recent study by Busche and colleagues used two-photon imaging to show that anti-amyloidogenic treatment in TG2576 and PDAPP mice did not recover neuronal hyperactivity but instead exacerbated it [33]. A major difference with the current study is that both models were treated either after the appearance of Aβ plaques, or using a single acute administration instead of a more chronic treatment regimen. These observations suggest that early stage hypersynchrony of BOLD FC might be recovered, in contrast to later stages. Our data suggests that the emphasis of treatment studies should be shifted to preventive strategies focusing on pre-plaque stage pathological Aβ, rather than removing Aβ plaques. These findings are also extremely important as Quiroz and colleagues made similar observations of increased BOLD FC in children

carrying the PSEN1 gene mutation. Chronic treatment protocols might provide more insight into how long the effects on BOLD FC can be delayed.

Additionally, early treatment with the 3D6 antibody recovered synaptic impairments. At 5 months, TG2576 mice showed a reduced paired-pulse ratio, which is indicative of changed presynaptic short-term plasticity [34]. This type of synaptic plasticity is thought to allow neurons to detect input coherence, to maintain stability and to promote synchronization [35,36]. In addition, it has been shown to play a vital role in important brain functions such as decision making, working memory and spatial place learning [37-39]. Treatment of TG2576 mice with 3D6 rendered the paired pulse ratio comparable to wild-types. Another indication for pre-synaptic alterations is the observation of increased expression of the pre-synaptic marker synapsin in TG2576 mice. Studies have demonstrated that low levels of Aβ enhance synaptic excitation at the pre-synaptic level [40,41]. Another possible explanation is a form of compensatory response for a loss of synaptic plasticity. Finally, hypersynchronous firing of neurons has been associated with remodeling of excitatory and inhibitory synapses [12,22]. Consistent with those findings, our data show an increased ratio of VGLUT1/GAD65-67 synapses and glutamate/GABA neurotransmitters in TG2576 mice, which were rescued in TG2576 mice treated with 3D6.

In conclusion, our data strongly suggest that early stages of AD progression are associated with hypersynchronous BOLD FC patterns, before the presence of Aβ plaques. These results provide more insight into the earliest changes that occur in AD, and might thus be of interest in terms of early biomarkers. Since aberrant BOLD FC patterns were demonstrated using rsfMRI, a non-invasive in vivo imaging technique that is already being used extensively in clinical studies, our data potentially holds high translational value. Moreover, our data suggest that this hypersynchronous FC can be rescued at an early stage, as anti-amyloidogenic treatment prevented hypersynchrony of BOLD FC, suggesting that preventive strategies should be the focus of future treatment studies.

Reference List

1. Kumar A, Singh A, Ekavali (2015) A review on Alzheimer's disease pathophysiology and its management: an update. Pharmacol Rep 67: 195-203.
2. Barage SH, Sonawane KD (2015) Amyloid cascade hypothesis: Pathogenesis and therapeutic strategies in Alzheimer's disease. Neuropeptides.
3. Hardy JA, Higgins GA (1992) Alzheimer's disease: the amyloid cascade hypothesis. Science 256: 184-185.
4. Mucke L, Selkoe DJ (2012) Neurotoxicity of amyloid beta-protein: synaptic and network dysfunction. Cold Spring Harb Perspect Med 2: a006338.
5. Dodart JC, Meziane H, Mathis C, Bales KR, Paul SM, et al. (1999) Behavioral disturbances in transgenic mice overexpressing the V717F beta-amyloid precursor protein. Behav Neurosci 113: 982-990.
6. Kishimoto Y, Higashihara E, Fukuta A, Nagao A, Kirino Y (2013) Early impairment in a water-finding test in a longitudinal study of the Tg2576 mouse model of Alzheimer's disease. Brain Res 1491: 117-126.
7. Kobayashi DT, Chen KS (2005) Behavioral phenotypes of amyloid-based genetically modified mouse models of Alzheimer's disease. Genes Brain Behav 4: 173-196.
8. Larson J, Lynch G, Games D, Seubert P (1999) Alterations in synaptic transmission and long-term potentiation in hippocampal slices from young and aged PDAPP mice. Brain Res 840: 23-35.
9. Rowan MJ, Klyubin I, Cullen WK, Anwyl R (2003) Synaptic plasticity in animal models of early Alzheimer's disease. Philos Trans R Soc Lond B Biol Sci 358: 821-828.
10. Moechars D, Dewachter I, Lorent K, Reverse D, Baekelandt V, et al. (1999) Early phenotypic changes in transgenic mice that overexpress different mutants of amyloid precursor protein in brain. J Biol Chem 274: 6483-6492.
11. Jacobsen JS, Wu CC, Redwine JM, Comery TA, Arias R, et al. (2006) Early-onset behavioral and synaptic deficits in a mouse model of Alzheimer's disease. Proc Natl Acad Sci U S A 103: 5161-5166.
12. Busche MA, Chen X, Henning HA, Reichwald J, Staufenbiel M, et al. (2012) Critical role of soluble amyloid-beta for early hippocampal hyperactivity in a mouse model of Alzheimer's disease. Proc Natl Acad Sci U S A 109: 8740-8745.
13. Biswal B, Yetkin FZ, Haughton VM, Hyde JS (1995) Functional connectivity in the motor cortex of resting human brain using echo-planar MRI. Magn Reson Med 34: 537-541.
14. Sheline YI, Raichle ME (2013) Resting state functional connectivity in preclinical Alzheimer's disease. Biol Psychiatry 74: 340-347.
15. Shah D, Jonckers E, Praet J, Vanhoutte G, Delgado YPR, et al. (2013) Resting state FMRI reveals diminished functional connectivity in a mouse model of amyloidosis. PLoS One 8: e84241.
16. Hsiao K, Chapman P, Nilsen S, Eckman C, Harigaya Y, et al. (1996) Correlative memory deficits, Abeta elevation, and amyloid plaques in transgenic mice. Science 274: 99-102.
17. Games D, Adams D, Alessandrini R, Barbour R, Berthelette P, et al. (1995) Alzheimer-type neuropathology in transgenic mice overexpressing V717F beta-amyloid precursor protein. Nature 373: 523-527.
18. Praet J, Reekmans K, Lin D, De Vocht N, Bergwerf I, et al. (2012) Cell type-associated differences in migration, survival, and immunogenicity following grafting in CNS tissue. Cell Transplant 21: 1867-1881.
19. Balschun D, Wolfer DP, Bertocchini F, Barone V, Conti A, et al. (1999) Deletion of the ryanodine receptor type 3 (RyR3) impairs forms of synaptic plasticity and spatial learning. EMBO J 18: 5264-5273.

20. Shah D, Deleye S, Verhoye M, Staelens S, Van der Linden A (2015) Resting-state functional MRI and [18F]-FDG PET demonstrate differences in neuronal activity between commonly used mouse strains. Neuroimage 125: 571-577.
21. Dodart JC, Mathis C, Bales KR, Paul SM, Ungerer A (1999) Early regional cerebral glucose hypometabolism in transgenic mice overexpressing the V717F beta-amyloid precursor protein. Neurosci Lett 277: 49-52.
22. Busche MA, Eichhoff G, Adelsberger H, Abramowski D, Wiederhold KH, et al. (2008) Clusters of hyperactive neurons near amyloid plaques in a mouse model of Alzheimer's disease. Science 321: 1686-1689.
23. Busche MA, Konnerth A (2015) Neuronal hyperactivity--A key defect in Alzheimer's disease? Bioessays 37: 624-632.
24. Bezzina C, Verret L, Juan C, Remaud J, Halley H, et al. (2015) Early onset of hypersynchronous network activity and expression of a marker of chronic seizures in the Tg2576 mouse model of Alzheimer's disease. PLoS One 10: e0119910.
25. Grandjean J, Schroeter A, He P, Tanadini M, Keist R, et al. (2014) Early alterations in functional connectivity and white matter structure in a transgenic mouse model of cerebral amyloidosis. J Neurosci 34: 13780-13789.
26. Quiroz YT, Schultz AP, Chen K, Protas HD, Brickhouse M, et al. (2015) Brain Imaging and Blood Biomarker Abnormalities in Children With Autosomal Dominant Alzheimer Disease: A Cross-Sectional Study. JAMA Neurol.
27. Johnson-Wood K, Lee M, Motter R, Hu K, Gordon G, et al. (1997) Amyloid precursor protein processing and A beta42 deposition in a transgenic mouse model of Alzheimer disease. Proc Natl Acad Sci U S A 94: 1550-1555.
28. Bard F, Cannon C, Barbour R, Burke RL, Games D, et al. (2000) Peripherally administered antibodies against amyloid beta-peptide enter the central nervous system and reduce pathology in a mouse model of Alzheimer disease. Nat Med 6: 916-919.
29. Demattos RB, Lu J, Tang Y, Racke MM, Delong CA, et al. (2012) A plaque-specific antibody clears existing beta-amyloid plaques in Alzheimer's disease mice. Neuron 76: 908-920.
30. Bard F, Fox M, Friedrich S, Seubert P, Schenk D, et al. (2012) Sustained levels of antibodies against Abeta in amyloid-rich regions of the CNS following intravenous dosing in human APP transgenic mice. Exp Neurol 238: 38-43.
31. Zago W, Buttini M, Comery TA, Nishioka C, Gardai SJ, et al. (2012) Neutralization of soluble, synaptotoxic amyloid beta species by antibodies is epitope specific. J Neurosci 32: 2696-2702.
32. Shankar GM, Li S, Mehta TH, Garcia-Munoz A, Shepardson NE, et al. (2008) Amyloid-beta protein dimers isolated directly from Alzheimer's brains impair synaptic plasticity and memory. Nat Med 14: 837-842.
33. Busche MA, Grienberger C, Keskin AD, Song B, Neumann U, et al. (2015) Decreased amyloid-beta and increased neuronal hyperactivity by immunotherapy in Alzheimer's models. Nat Neurosci.
34. Zucker RS, Regehr WG (2002) Short-term synaptic plasticity. Annu Rev Physiol 64: 355-405.
35. Blackman AV, Abrahamsson T, Costa RP, Lalanne T, Sjostrom PJ (2013) Target-cell-specific short-term plasticity in local circuits. Front Synaptic Neurosci 5: 11.
36. Dutta Roy R, Stefan MI, Rosenmund C (2014) Biophysical properties of presynaptic short-term plasticity in hippocampal neurons: insights from electrophysiology, imaging and mechanistic models. Front Cell Neurosci 8: 141.
37. Silva AJ, Giese KP, Fedorov NB, Frankland PW, Kogan JH (1998) Molecular, cellular, and neuroanatomical substrates of place learning. Neurobiol Learn Mem 70: 44-61.
38. Silva AJ, Rosahl TW, Chapman PF, Marowitz Z, Friedman E, et al. (1996) Impaired learning in mice with abnormal short-lived plasticity. Curr Biol 6: 1509-1518.
39. Deng PY, Klyachko VA (2011) The diverse functions of short-term plasticity components in synaptic computations. Commun Integr Biol 4: 543-548.

40. Palop JJ, Mucke L (2010) Amyloid-beta-induced neuronal dysfunction in Alzheimer's disease: from synapses toward neural networks. Nat Neurosci 13: 812-818.
41. Abramov E, Dolev I, Fogel H, Ciccotosto GD, Ruff E, et al. (2009) Amyloid-beta as a positive endogenous regulator of release probability at hippocampal synapses. Nat Neurosci 12: 1567-1576.

Acknowledgments

The authors wish to thank Elien Theuns (Laboratory of Cell Biology and Histology, University of Antwerp) and Tim Willems (Department of Biology, University of Antwerp) for technical assistance. This research was supported by the European Union's Seventh Framework Programme under grant agreement number 278850 (INMiND), by Molecular Imaging of Brain Pathophysiology (BRAINPATH) under grant agreement number 612360 within the Marie Curie Actions-Industry-Academia Partnerships and Pathways (IAPP) program, by the Institute for the Promotion of Innovation by Science and Technology (IWT) in Flanders, and by the Fund for Scientific Research Flanders (FWO) (grant agreement G.0D76.14, G.0587.14.). DS is holder of an IWT PhD grant (grant agreement 13160). JP is holder of an FWO postdoc grant (grand agreement 12G1416N). JRD is holder of an IWT Baekeland grant (grand agreement 140775). Aspects of this work were supported by funding to S.R. from the German Research Council (DFG, grant # RO 2226/13-1) and from the JPND CrossSeeds consortium (BMBF, grant # 01ED1501B).

Keywords

Amyloidosis; Alzheimer’s disease; transgenic mouse models; BOLD functional connectivity; resting-state fMRI; hypersynchrony; TG2576; PDAPP.

Figure legends

Figure 1: BOLD FC matrices in the TG2576 mouse model at pre-plaque and post-plaque stages. This figure shows mean FC strength matrices of wild-type (WT) (lower half) vs. TG2576 (upper half) mice. The BOLD FC-matrices show functional correlation strengths between pairs of brain regions at 3, 5, 8 (pre-plaque stages) and 14 and 18 (post-plaque stages) months of age. The colour scale represents the strength of the functional correlation. The different brain ROIs and their abbreviations are listed in **Supplementary Table 1**.

Figure 2: The earliest signs of hypersynchronous BOLD FC are observed in the hippocampus network. A) mean BOLD FC strength is shown per brain network for wild-type vs. TG2576 mice at 3 and 5 months of age. **B)** mean BOLD FC strength of the hippocampus is shown for all age groups in wild-type and TG2576 mice. * p-value<0.05, ** p-value<0.01, *** p-value<0.001. All values are presented as mean ± standard error. **C)** three axial slices of the mean statistical hippocampus zFC-maps for 5 months old wild-type and TG2576 mice are shown as an overlay on an anatomical T2-weighted MRI image. The positioning of the slices is shown on a coronal brain image. The zFC-maps are additionally shown on a 3D-rendering. The colour scale represents the T-value i.e. the strength of functional correlation with the right hippocampus.

Figure 3: Inflammation, Aβ load and electrophysiology in the hippocampus of TG2576 mice at 5 months of age. A) mean % area GFAP and Iba1 for wild-type and TG2576 mice. One representative image of a wild-type and TG2576 animal is shown for each staining (scale bar indicates 100μm). **B)** mean mRNA expression (fold wild-type) of qPCR markers of inflammation for wild-type and TG2576 mice . **C)** mean % area thioflavin-S (left y-axis) and mean soluble Aβ (pg/ml brain homogenate) (right y-axis) for wild-type and TG2576 mice. **D)** input/output (I/O) curve represented as mean field EPSP (V/s) for wild-type and TG2576 mice. **E)** Paired pulse facilitation (PPF) is shown as the mean PPF ratio at different inter stimulus intervals (ISI) for wild-type and TG2576 mice. **F)** Long term potentiation (LTP) represented as the mean field EPSP slope (% of baseline) for wild-type and TG2576 mice. * p-value<0.05. All values are presented as mean ± standard error.

Figure 4: FC strength increases in the PDAPP mouse model vs. wild-types at a pre-plaque stage. **A)** mean FC-matrices of the wild-type (WT) (lower half) and PDAPP (upper half) mice show functional correlation strengths between pairs of brain regions. The colour scale represents the strength of the functional correlation. The different brain ROIs and their abbreviations are listed in **Supplementary Table 1**. **B)** mean BOLD FC strength per brain network for wild-type and PDAPP mice. **C)** mean BOLD FC of the frontal network at 3, 5 and 7 months of age in wild-type and PDAPP mice. **D)** mean % area thioflavin-S (left y-axis) and mean soluble Aβ (pg/ml brain homogenate) (right y-axis) in the frontal cortex for wild-type and PDAPP mice. * p-value<0.05, ** p-value<0.01. All values are presented as mean ± standard error.

Figure 5: Early treatment with 3D6 restores FC abnormalities in TG2576 mice at a pre-plaque stage. A) mean FC strength matrices of wild-type (WT) (lower half) vs. TG2576 (upper half) mice after treatment with PBS or 3D6. The FC-matrices show functional correlation strengths between pairs of brain regions. The colour scale represents the strength of the functional correlation. The different brain ROIs and their abbreviations are listed in **Supplementary Table 1**. **B)** Three axial slices of the mean statistical hippocampus zFC-maps are shown for PBS treated wild-type and TG2576 mice, and 3D6 treated wild-type and TG2576 mice at 5 months. ZFC-maps are shown as an overlay on an anatomical T2-weighted MRI image. The positioning of the slices is shown on a coronal brain image. The zFC-maps are additionally shown on a 3D-rendering. The colour scale represents the T-value i.e. the strength of functional correlation with the right hippocampus.

Figure 6: Treatment with 3D6 prevents FC and synaptic abnormalities in the hippocampus network in 5 months old TG2576 mice. A) mean BOLD FC strength in the hippocampus network for PBS treated wild-types and TG2576 mice, and 3D6 treated wild-types and TG2576 mice at 3, 5, 7, 8 and 10 months of age. The green box indicates the start of the 3D6 treatment regimen (at 3 months of age) and the red box the end (at 5 months of age). **B)** mean PPF ratio at different inter stimulus intervals (ISI) for PBS treated wild-types and TG2576 mice, and 3D6 treated wild-types and TG2576 mice at 5 months of age. **C)** mean density VGLUT1 (left y-axis), mean density GAD65-67 (left y-axis) and mean VGLUT1/GAD65-67 ratio (right y-axis) for PBS treated wild-types and TG2576 mice, and 3D6 treated wild-types and TG2576 mice at 5 months of age. One representative image is shown for each group (VGLUT1 red, GAD65/67 green, scale bar indicates 8µm). The upper panel shows immunofluorescent images, the lower panel shows tresholded images. **D)** mean glutamate/GABA ratio for PBS treated wild-types and TG2576 mice, and 3D6 treated wild-types and TG2576 mice at 5 months of age. **E)** mean density synapsin and synaptobrevin for PBS treated wild-types and TG2576 mice, and 3D6 treated wild-types and TG2576 mice at 5 months of age. One representative image is shown for each group (synapsin red, synaptobrevin green, scale bar indicates 8µm). The upper panel shows immunofluorescent images, the lower panel shows thresholded images. * p-value<0.05, ** p-value<0.01, *** p-value<0.001. All values are presented as mean ± standard error.

Figure 1:

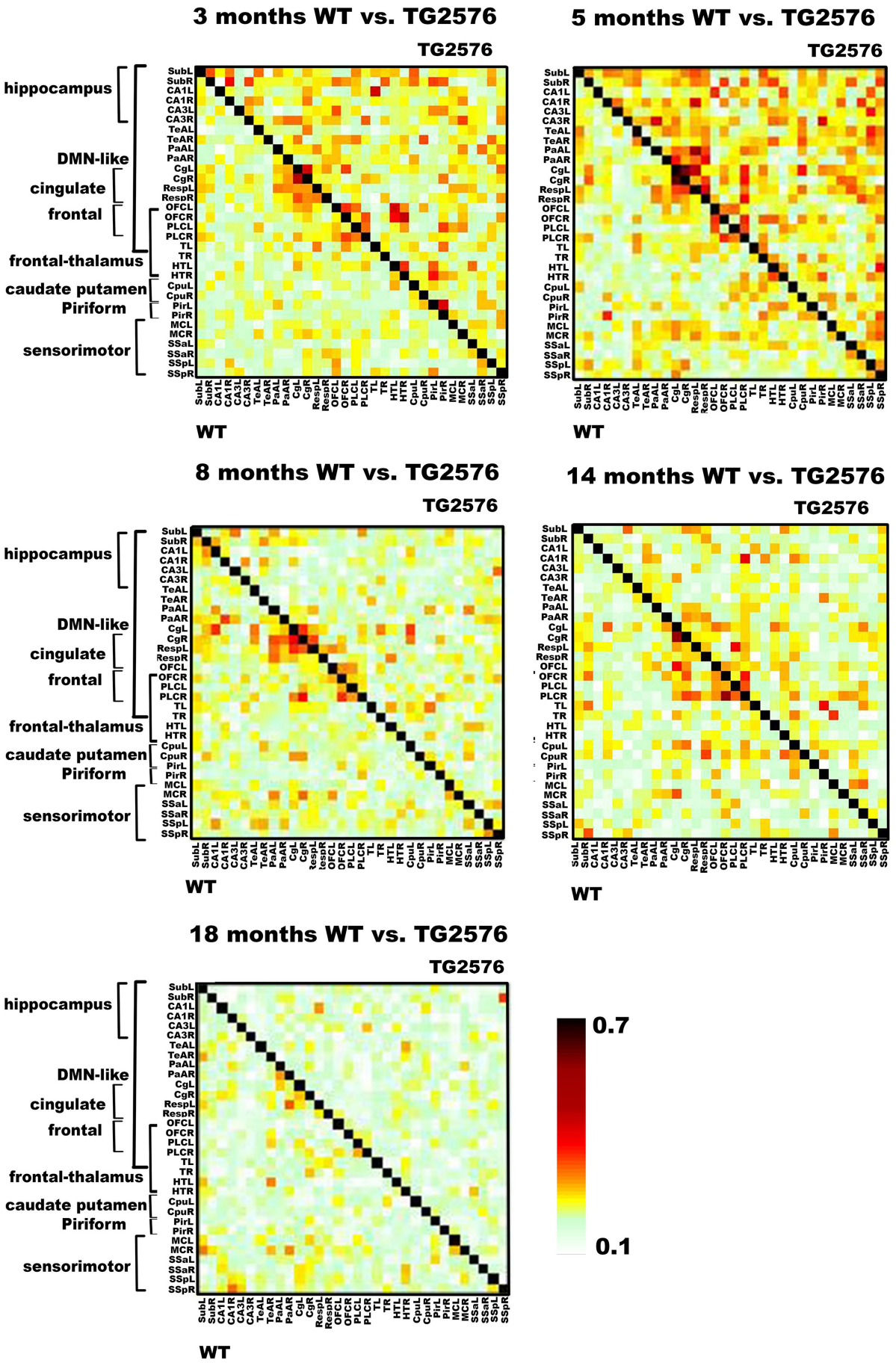
3 months WT vs. TG2576
TG2576
WT
5 months WT vs. TG2576
TG2576
WT
8 months WT vs. TG2576
TG2576
WT
14 months WT vs. TG2576
TG2576
WT
18 months WT vs. TG2576
TG2576
WT
hippocampus
DMN-like
cingulate
frontal
frontal-thalamus
caudate putamen
Piriform
sensorimotor
SubL
SubR
CA1L
CA1R
CA3L
CA3R
TeAL
TeAR
PaAL
PaAR
CgL
CgR
RespL
RespR
OFCL
OFCR
PLCL
PLCR
TL
TR
HTL
HTR
CpuL
CpuR
PirL
PirR
MCL
MCR
SSaL
SSaR
SSpL
SSpR
0.7
0.1

Figure 2:

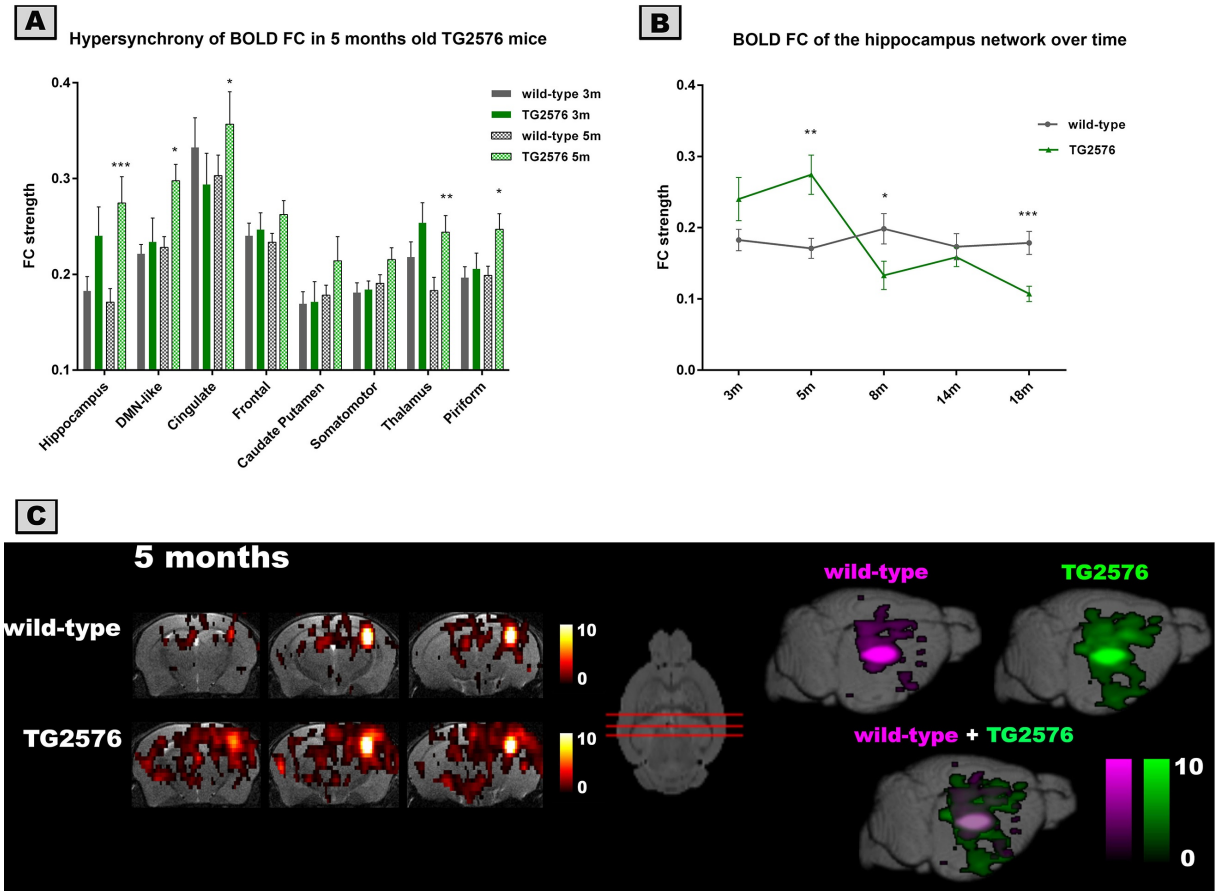
A
Hypersynchrony of BOLD FC in 5 months old TG2576 mice
FC strength
wild-type 3m
TG2576 3m
wild-type 5m
TG2576 5m
Hippocampus
DMN-like
Cingulate
Frontal
Caudate Putamen
Somatomotor
Thalamus
Piriform
B
BOLD FC of the hippocampus network over time
FC strength
wild-type
TG2576
3m
5m
8m
14m
18m
C
5 months
wild-type
TG2576
10
0
wild-type
TG2576
wild-type + TG2576
10
0

Figure 3:

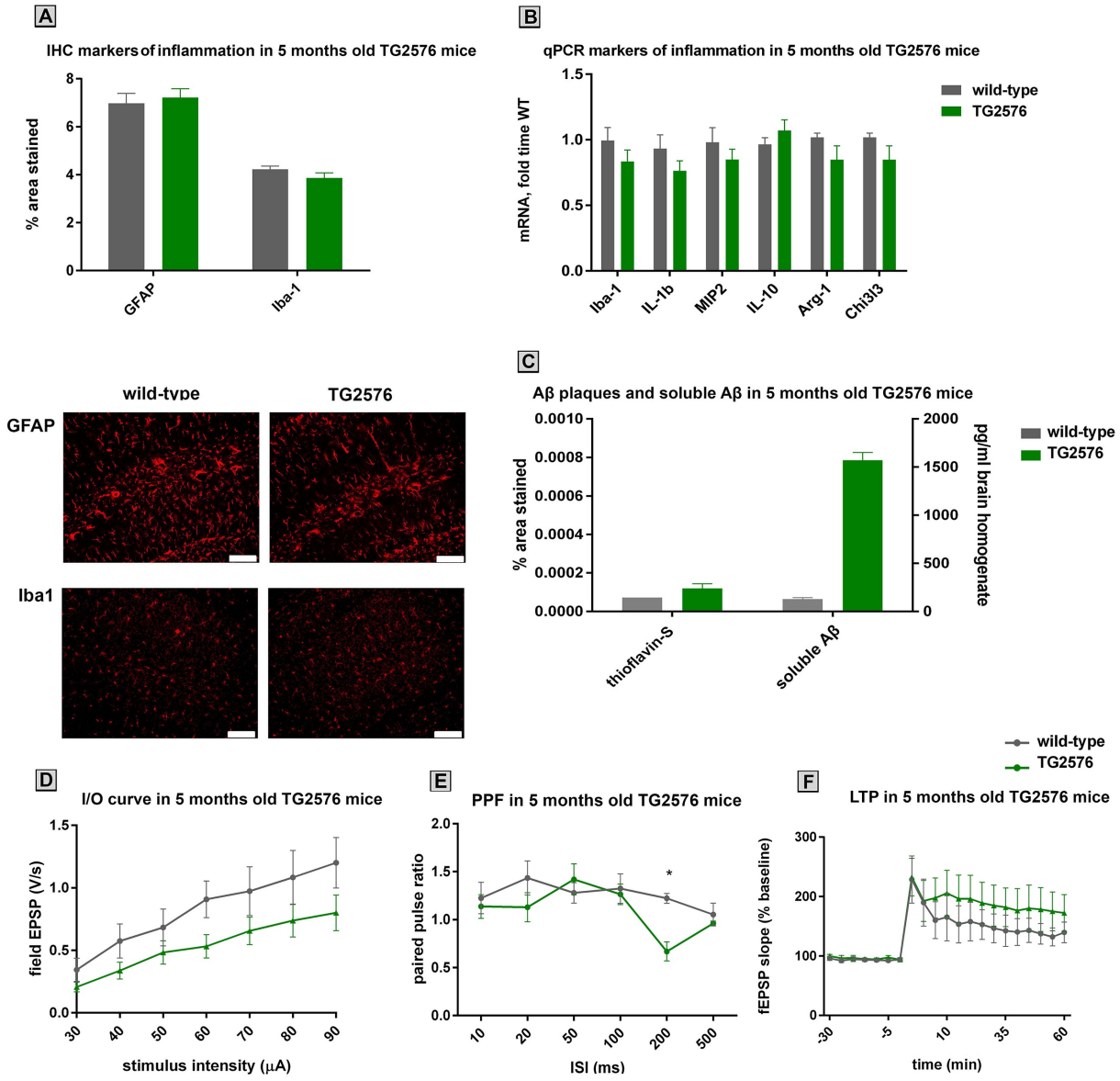
A
IHC markers of inflammation in 5 months old TG2576 mice
% area stained
GFAP
Iba-1
B
qPCR markers of inflammation in 5 months old TG2576 mice
mRNA, fold time WT
wild-type
TG2576
Iba-1
IL-1b
MIP2
IL-10
Arg-1
Chi3l3
wild-type
TG2576
GFAP
Iba1
C
Aβ plaques and soluble Aβ in 5 months old TG2576 mice
% area stained
pg/ml brain homogenate
thioflavin-S
soluble Aβ
wild-type
TG2576
D
I/O curve in 5 months old TG2576 mice
field EPSP (V/s)
stimulus intensity (μA)
E
PPF in 5 months old TG2576 mice
paired pulse ratio
ISI (ms)
F
LTP in 5 months old TG2576 mice
fEPSP slope (% baseline)
time (min)
wild-type
TG2576

Figure 4:

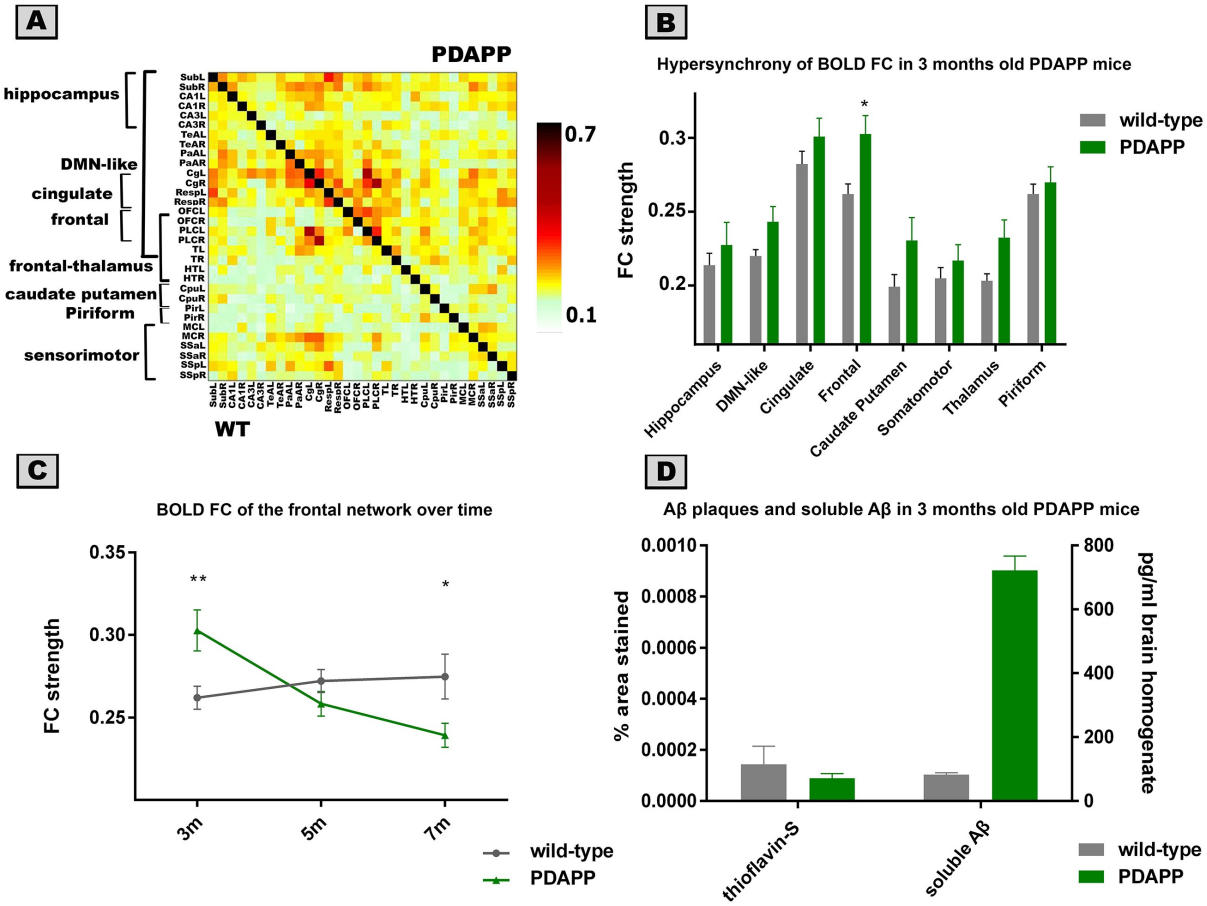
A
PDAPP
hippocampus
DMN-like
cingulate
frontal
frontal-thalamus
caudate putamen
Piriform
sensorimotor
0.7
0.1
WT
B
Hypersynchrony of BOLD FC in 3 months old PDAPP mice
FC strength
wild-type
PDAPP
Hippocampus
DMN-like
Cingulate
Frontal
Caudate Putamen
Somatomotor
Thalamus
Piriform
C
BOLD FC of the frontal network over time
FC strength
3m
5m
7m
wild-type
PDAPP
D
Aβ plaques and soluble Aβ in 3 months old PDAPP mice
% area stained
pg/ml brain homogenate
thioflavin-S
soluble Aβ
wild-type
PDAPP

Figure 5:

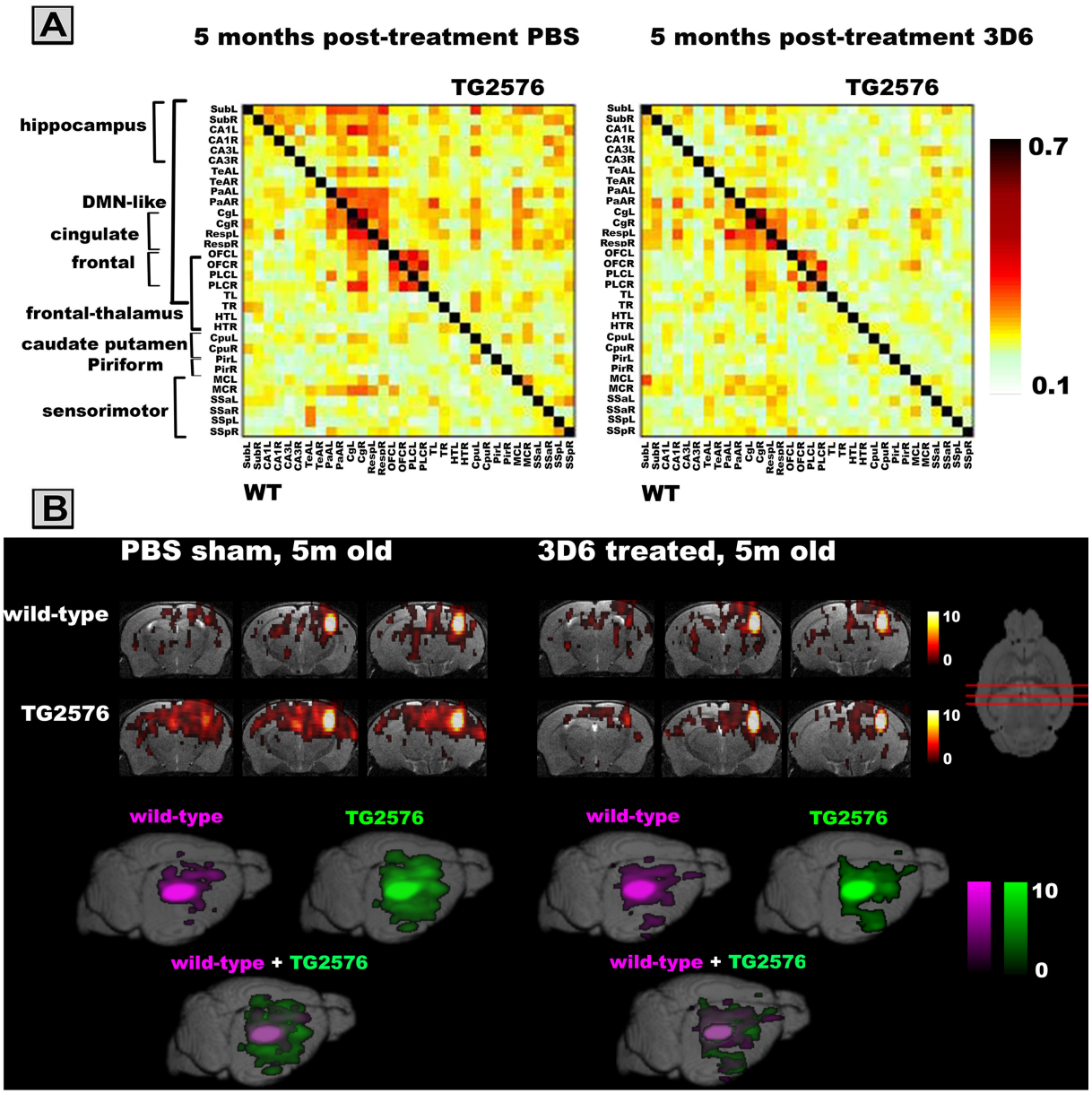
A
5 months post-treatment PBS
5 months post-treatment 3D6
TG2576
TG2576
hippocampus
DMN-like
cingulate
frontal
frontal-thalamus
caudate putamen
Piriform
sensorimotor
SubL SubR CA1L CA1R CA3L CA3R TeAL TeAR PaAL PaAR CgL CgR RespL RespR OFCL OFCR PLCL PLCR TL TR HTL HTR CpuL CpuR PirL PirR MCL MCR SSaL SSaR SSpL SSpR
0.7
0.1
WT
WT
B
PBS sham, 5m old
3D6 treated, 5m old
wild-type
TG2576
10
0
wild-type
TG2576
wild-type + TG2576
wild-type + TG2576
10
0

Figure 6:

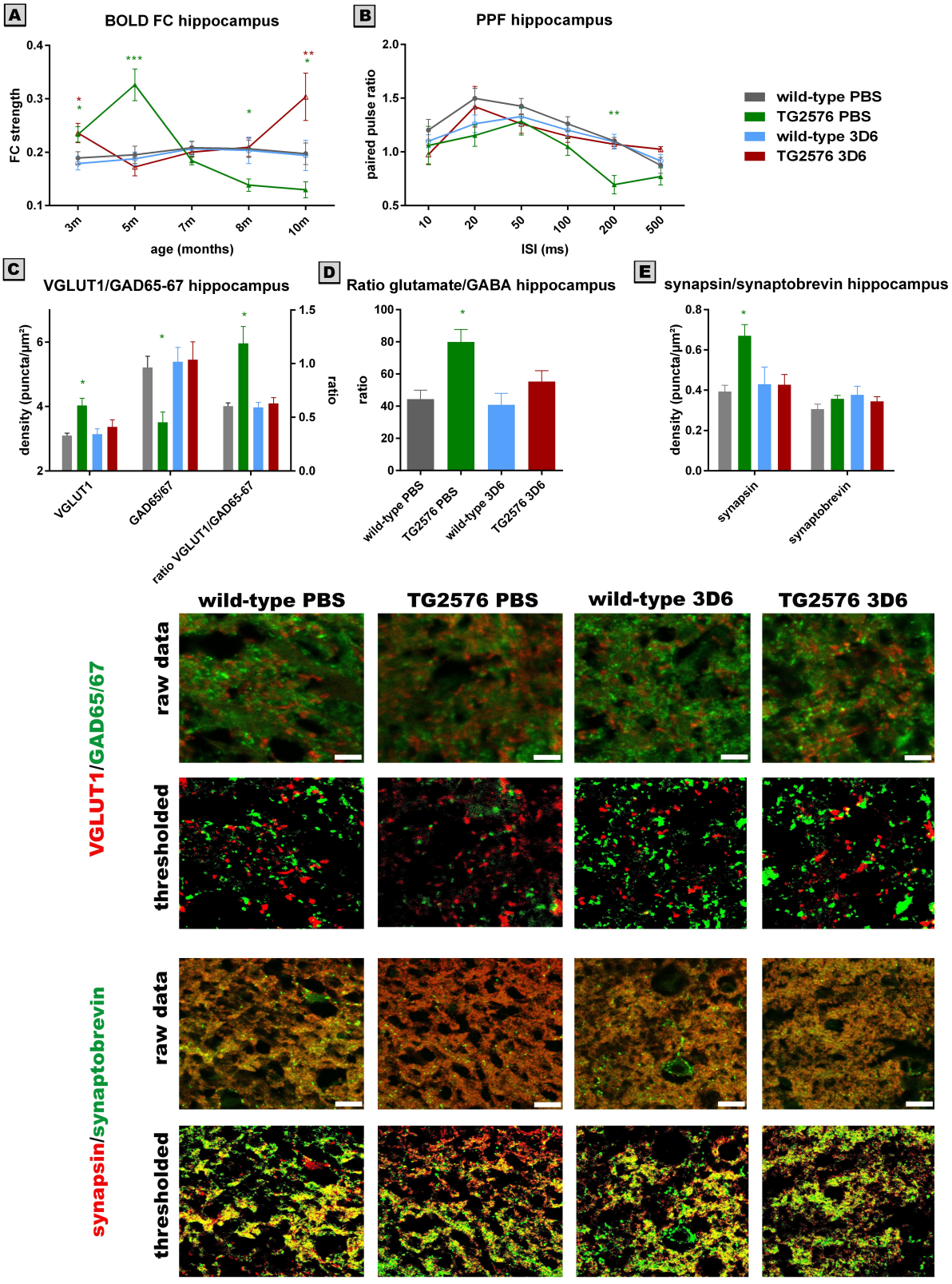
A
BOLD FC hippocampus
FC strength
age (months)
3m
5m
7m
8m
10m
B
PPF hippocampus
paired pulse ratio
ISI (ms)
10
20
50
100
200
500
wild-type PBS
TG2576 PBS
wild-type 3D6
TG2576 3D6
C
VGLUT1/GAD65-67 hippocampus
density (puncta/µm²)
ratio
VGLUT1
GAD65/67
ratio VGLUT1/GAD65-67
D
Ratio glutamate/GABA hippocampus
ratio
E
synapsin/synaptobrevin hippocampus
density (puncta/µm²)
synapsin
synaptobrevin
wild-type PBS
TG2576 PBS
wild-type 3D6
TG2576 3D6
VGLUT1/GAD65/67
raw data
thresholded
synapsin/synaptobrevin
raw data
thresholded